Taylor & Francis
Taylor & Francis Group

RESEARCH PAPER

🔓 OPEN ACCESS ⬤ Check for updates

Benzoxazole derivatives as new VEGFR-2 inhibitors and apoptosis inducers: design, synthesis, *in silico* studies, and antiproliferative evaluation

Mohammed S. Taghour[a], Hazem A. Mahdy[a] (iD), Maher H. Gomaa[b], Ahmed Aglan[b], Mahmoud Gomaa Eldeib[b], Alaa Elwan[a], Mohammed A. Dahab[a], Eslam B. Elkaeed[c], Aisha A. Alsfouk[d] (iD), Mohamed M. Khalifa[a] (iD), Ibrahim H. Eissa[a] (iD) and Hazem Elkady[a]

aPharmaceutical Medicinal Chemistry & Drug Design Department, Faculty of Pharmacy (Boys), Al-Azhar University, Cairo, Egypt; bBiochemistry and Molecular Biology Department, Faculty of Pharmacy (Boys), Al-Azhar University, Cairo, Egypt; cDepartment of Pharmaceutical Organic Chemistry, Faculty of Pharmacy (Boys), Al-Azhar University, Cairo, Egypt; dDepartment of Pharmaceutical Sciences, College of Pharmacy, Princess Nourah bint Abdulrahman University, Riyadh, Saudi Arabia

ABSTRACT

In this study, a set of novel benzoxazole derivatives were designed, synthesised, and biologically evaluated as potential VEGFR-2 inhibitors. Five compounds (**12d**, **12f**, **12i**, **12l**, and **13a**) displayed high growth inhibitory activities against HepG2 and MCF-7 cell lines and were further investigated for their VEGFR-2 inhibitory activities. The most potent anti-proliferative member **12l** ($IC_{50} = 10.50\,\mu M$ and $15.21\,\mu M$ against HepG2 and MCF-7, respectively) had the most promising VEGFR-2 inhibitory activity ($IC_{50} = 97.38\,nM$). A further biological evaluation revealed that compound **12l** could arrest the HepG2 cell growth mainly at the Pre-G1 and G1 phases. Furthermore, compound **12l** could induce apoptosis in HepG2 cells by 35.13%. likely, compound **12l** exhibited a significant elevation in caspase-3 level (2.98-fold) and BAX (3.40-fold), and a significant reduction in Bcl-2 level (2.12-fold). Finally, docking studies indicated that **12l** exhibited interactions with the key amino acids in a similar way to sorafenib.

1. Introduction

Cancer chemotherapy has been considered one of the most important medical advances in the past few decades[1]. However, the narrow therapeutic index besides the unpredictable effects were the major drawbacks of the primary introduced drugs[2]. In contrast, the recently developed targeted therapies gained the advantages of interfering with specific molecular targets almost located in the tumour cells with minimised effect on the normal cells[3]. Thus, these agents provide a high specific therapeutic window with limited non-specific toxicities.

Among the major vital cancer drug targets are tyrosine kinases (TKs) because of their potential role in the modulation of growth factor signalling[4,5]. Upon their activation, TKs increase both proliferation and growth of tumour cells with induction of apoptosis and reinforcement of angiogenesis and metastasis[6]. Thus, TKs inhibition by different inhibitors became a key approach in cancer management[7]. The evidenced drug ability as well as the safety profile of the FDA-approved TKs inhibitors emphasised the attractiveness of TKs as drug targets.

Owing to their significant participation in modulating angiogenesis, vascular endothelial growth factors (VEGFs) have been considered the key players over other TKs[8]. VEGFs action is performed after their binding to three different tyrosine kinase (TK) receptors, namely, VEGFR-1, VEGFR-2, and VEGFR-3[8]. VEGFR-2 receptor possesses the most crucial role among the rest subtypes

as its activation leads to initiation of downstream signal transduction pathway *via* dimerisation followed by autophosphorylation of tyrosine receptor, a pathway resulting finally to angiogenesis[9]. Therefore, hindering VEGF/VEGFR-2 pathway or, even, weakening its response is of considered targets of the recent chemotherapeutic agents[10]. Despite a large number of small molecules with various chemical scaffolds being evidenced to tackle this pathway, resistance development in addition to different adverse effects still the main drawback of the current known VEGFR-2 inhibitors drugs[11]. Thus, the discovery of more effective and less dangerous VEGFR-2 inhibitors becomes an attractive therapeutic target for cancer drug discovery[12]. It has been discovered that VEGFR-2 inhibition in cancer cells causes and expedites apoptosis, which works in concert to enhance the antitumor effect. Hence, the most potent derivative has thoroughly discoursed in our work through the assessment of certain apoptotic markers such as caspase-3 (a crucial component in apoptosis that coordinates the destruction of cellular structures such as DNA and cytoskeletal proteins[13], BAX and Bcl-2 (members of the Bcl-2 family and core regulators of the intrinsic pathway of apoptosis)[14].

Over the last decade, we have built a project that is concerned with cancer management. Our high-throughput efforts gave us the opportunity to identify several small molecules that may serve as anti-angiogenic agents[9]. Most of these molecules exhibited VEGFR-2 inhibitory activity comparable to that of the FDA-approved
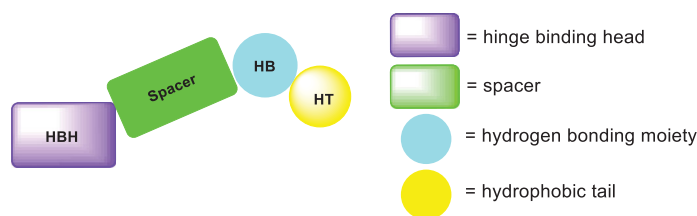
Figure 1. The four main pharmacophoric requirements of VEGFR-2 inhibitors.

inhibitor, sorafenib. These molecules were precisely designed to resemble the four main structural parts of sorafenib and other VEGFR-2 inhibitors[15–17]. Those parts were well-known to be a hydrophobic hinge binding head, a linker, a hydrogen-bonding moiety, and a hydrophobic tail (Figure 1). These previously mentioned parts enabled the designed compounds to fit perfectly in the TK active pocket. Based on the promising biological results in our former published work in which we utilised benzoxazole moieties as a hinge-binding core[18], we decided to continue our preliminary VEGFR-2 studies using the same three different scaffolds of benzoxazole but with two main considerable additional modifications; a) For the allosteric hydrophobic pocket, we used different terminal aliphatic hydrophobic moieties including cyclopentyl (compounds **12a-c**) and ter-butyl moiety (compounds **12d-f**). This allowed us to make a comparative study between aliphatic and aromatic derivatives of each scaffold and study the SAR of the obtained compounds as anticancer leads with significant VEGFR-2 inhibitory potentialities, as was planned in our design. b) The pharmacophore moiety was selected to be amide derivative (compounds **12a-l**) or diamide derivatives (compounds **13a-c**) to study which derivative is more preferred biologically.

1.1. Rationale and design

Forcing by the fact that molecular hybridisation is one of the most important drug discovery approaches, our team co-workers started the present work. Sunitinib, a multi-targeted receptor tyrosine kinase (RTK) inhibitor[19], lucitanib, a dual VEGFRs and FGFRs inhibitor[20], and compound **A**, a potent VEGFR-2 inhibitor were our guides for building a new anti-angiogenic hybrid[21]. Thus, the indolinylidene moiety of sunitinib was altered to be benzoxazole in the new hybrid to investigate its ability to modify the biological effects. In addition, we did another modification to the sunitinib structure *via* replacing the fluorine atom by either hydrogen, methyl, or chlorine atoms that allowed us to measure the biological effects of these atoms compared to the fluorine atom. In contrast, the carboxamide moiety of both sunitinib and lucitanib was kept or expanded to continue acting as a hydrogen bonding part. On the other side, the hydrophobic tail in the new hybrid was suggested to be either aliphatic (*tert*-butyl), alicyclic (cyclopentyl), or aromatic (methoxy or chloro phenyl) to get a diverse number of congeners with a higher chance to study the structure-activity relationship of the newly designed hybrid. However, an *in silico* study was also carried out through the docking tools to confirm the proposed design (Figure 2).

2. Results and discussion

2.1. Chemistry

The final benzoxazoles **12a-l** and **13a-c** were synthesised as presented in Schemes 1–3. The starting materials and key intermediates **2a-c**, **3a-c**, **5**, **6**, **7a-d**, **9**, **10,** and **11** were primarily prepared according to the reported methods[22–25] as delineated in Schemes 1 and 2.

The final target candidates **12a-l** and **13a-c** were furnished in dry DMF *via* heating the potassium salts **3a-c** with the previously synthesised intermediates **7a-d** and **11**, respectively (Scheme 3). Infra-red (IR) spectra of compounds **12a-l** indicated the presence of characteristic NH and C=O groups stretching bands at a range of 3181–3412 and 1644–1688 cm^{-1}, respectively. Moreover, their ^{1}H NMR spectra showed the presence of the two NH amide group signals at a range of δ 7.73–10.83 ppm. The formation of compounds **13a-c** was confirmed by ^{1}H NMR spectra which showed the appearance of three singlet signals at a range of δ 10.53–10.79 ppm corresponding to the NH protons.

2.2. Biological evaluation

2.2.1. In-vitro antiproliferative activities *against MCF-7 and HepG2 cell lines*

The *in vitro* antiproliferative effects of the newly synthesised benzoxazole derivatives **12a-l** and **13a-c** were determined against hepatocellular cancer (HepG2) and breast cancer (MCF-7) cell lines employing the standard MTT assay protocol wherein sorafenib was applied as a reference. The cytotoxicity results were obtained as median growth inhibitory concentration (IC$_{50}$). As presented in Table 1, major members of the synthesised compounds displayed promising anticancer activity.

Observing the results of anti-proliferative activity, valuable data concerning the structure-activity relationships was determined. In general, the 5-methylbenzo[*d*]oxazole containing derivatives (compounds **12c, 12f, 12i, 12 l,** and **13c**) (IC$_{50}$ values ranging from 10.50 to 74.30 μM) were more active than the unsubstituted benzo[*d*]oxazole derivatives (compounds **12a, 12d, 12 g, 12j,** and **13a**) (IC$_{50}$ values ranging from 25.47 to 53.01 μM). In the meantime, the 5-chlorobenzo[*d*]oxazole derivatives (compounds **12b, 12e, 12h, 12k,** and **13b**) (IC$_{50}$ values ranging from 26.31 to 102.10 μM) exhibited less potent activities.

A closer look to the results indicated that compound **12l** achieved the most potent anticancer activity against HepG2 and MCF-7 cell lines with IC$_{50}$ values of 10.50 μM and 15.21 μM, respectively, compared to sorafenib with IC$_{50}$ value of 5.57 μM and 6.46 μM against HepG2 and MCF-7, respectively. This indicated that hybridisation of 5-methylbenzo[*d*]oxazole with terminal 3-chlorophenyl moiety potentiates the anticancer activity against HepG2 and MCF-7 cell lines. Moreover, compounds **12d** (IC$_{50}$ = 23.61 and 44.09 μM), **12f** (IC$_{50}$ = 36.96 and 22.54 μM), **12i** and (IC$_{50}$ = 27.30 and 27.99 μM) exhibited promising activities against HepG2 and MCF-7 cell lines, respectively.

Initially, the effect of a hydrogen-bonding moiety on cytotoxic activities has been explored. Regarding the unsubstituted benzo[*d*]oxazole derivatives, it was noticed that the diamide derivative **13a** (IC$_{50}$ = 25.47 and 32.47 μM against HepG2 and MCF-7, respectively) displayed better effects than the corresponding amide derivative **12j** (IC$_{50}$ = 50.92 and 33.61 μM against MCF-7 and HepG2, respectively). Conversely, in 5-methylbenzo[*d*]oxazole derivatives, the decreased IC$_{50}$ value of the amide derivative **12l** (IC$_{50}$ = 10.50 μM and 15.21 μM against HepG2 and MCF-7, respectively) in comparison to the corresponding diamide member of the same scaffold **13c** (IC$_{50}$ = 24.25 and 53.13 μM) indicated that the amide derivatives more preferred biologically than the corresponding diamide derivatives.

We then investigated the impact of the terminal hydrophobic tail on the *in-vitro* antiproliferative activities. Concerning the unsubstituted benzo[*d*]oxazole derivatives, compound **12d**,
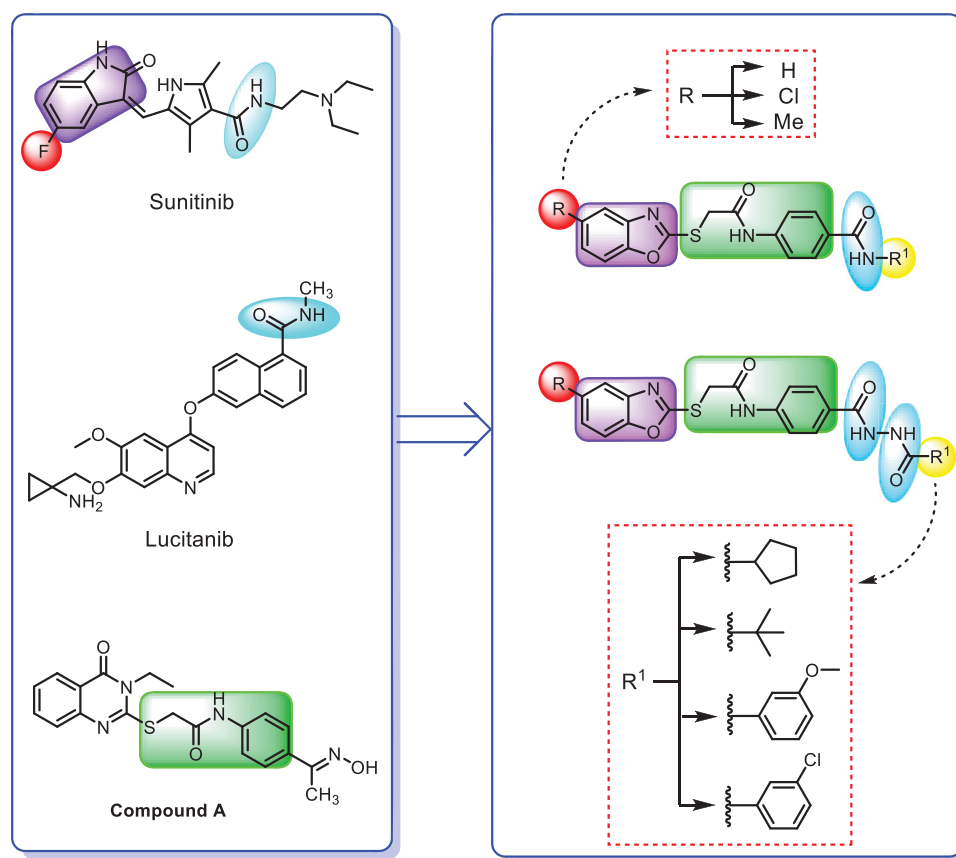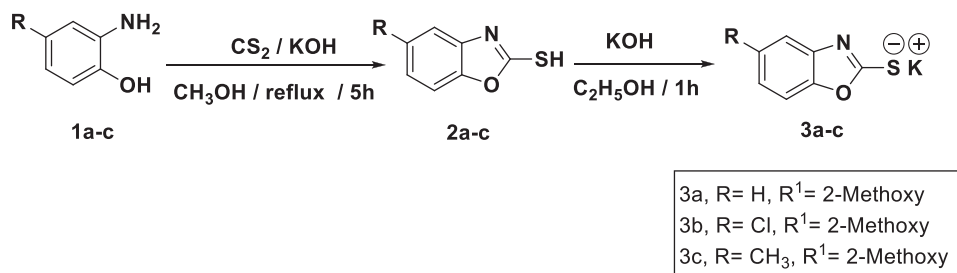
Figure 2. Summary of the suggested rationale.

3a, R= H, R^1= 2-Methoxy
3b, R= Cl, R^1= 2-Methoxy
3c, R= CH$_3$, R^1= 2-Methoxy

Scheme 1. Synthesis of the starting materials **3a-c**.

containing terminal *tert*-butyl moiety displayed the highest inhibitory activity against the HepG2 cell line with an IC$_{50}$ value of 23.61 μM while **13a,** containing terminal 3-chlorophenyl moiety exhibited the lowest IC$_{50}$ value (32.47 μM) against MCF-7 cell line. On the other hand, among 5-chlorobenzo[*d*]oxazole-based derivatives, the amide member bearing terminal 3-chlorophenyl arm **12k** displayed the most potent *in-vitro* antiproliferative activities against the HepG2 cell line with an IC$_{50}$ value of 28.36 μM. In the meantime, the diamide member **13 b,** bearing the same terminal arm presented the most promising activity against MCF-7 cell line with IC$_{50}$ value of 26.31 μM.

2.2.2. Vegfr-2 inhibitory assay

VEGFR-2 inhibitory effect of the most cytotoxic candidates **12d, 12f, 12i, 12 l,** and **13a** was investigated and summarised in Table 2. Sorafenib was used as a reference.

Matching with the cytotoxicity results, compound **12l,** the most cytotoxic member, displayed the strongest VEGFR-2 inhibitory effect (IC$_{50}$ = 97.38 nM) comparing sorafenib (IC$_{50}$ =

48.16 nM). Additionally, compounds **12d** and **12i** showed moderate VEGFR-2 inhibitory effects with the concentrations of 194.6 and 155 nM, respectively. Unlikely, compounds **12f** and **13a** showed weak VEGFR-2 effects with the concentration of 264.90 and 267.80 nM, respectively.

2.2.3. Correlation study between cytotoxicity and VEGFR-2 inhibition

The VEGFR-2 inhibitory activities of the tested compounds were plotted against their corresponding cytotoxicity in a simple linear regression for the HepG2 cell line in order to confirm the relationship between VEGFR-2 inhibition and cytotoxicity. The calculated R^2 square value 0.6274) shows a significant correlation between the tested compounds' induction of cytotoxicity and inhibition of VEGFR-2. As a result, one possible mechanism of the established compounds' cytotoxicity in the established cell line is their inhibition of VEGFR-2 activity (Figure 3).
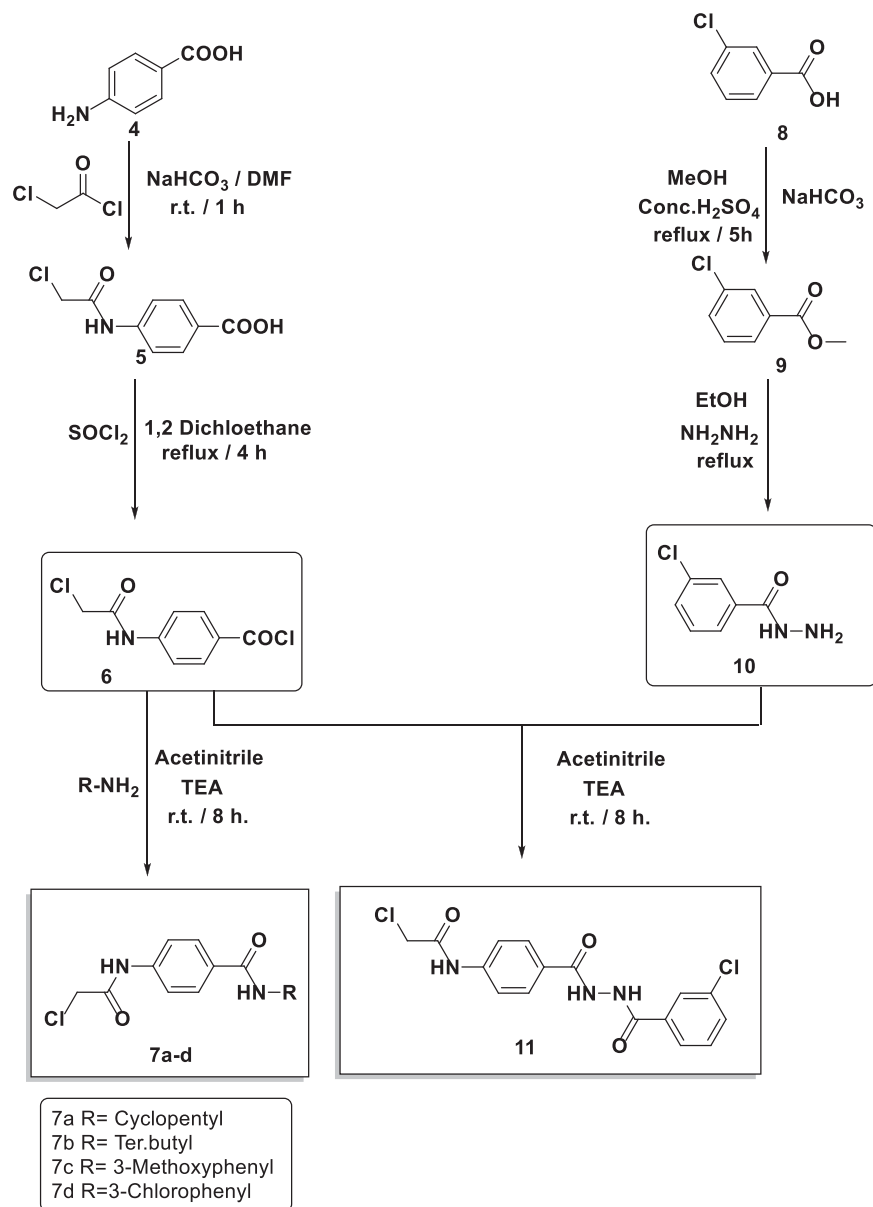
Scheme 2. Synthesis of the intermediates **7a-d** and **11**.

2.2.4. Evaluation of in vitro cytotoxicity against normal cell line

The most potent members **12d**, **12i**, and **12l** were assessed for their in vitro cytotoxicity against normal cell lines using WI-38 (a human lung cell line) and sorafenib as a reference The IC_{50} values for compounds **12d**, **12i**, and **12l** were 99.41, 76.78, and 37.97 M, respectively (Table 3). Such values were very high in comparison to the corresponding values on cancer cell lines, which reflect high safety profile of the tested candidates towards normal cell lines.
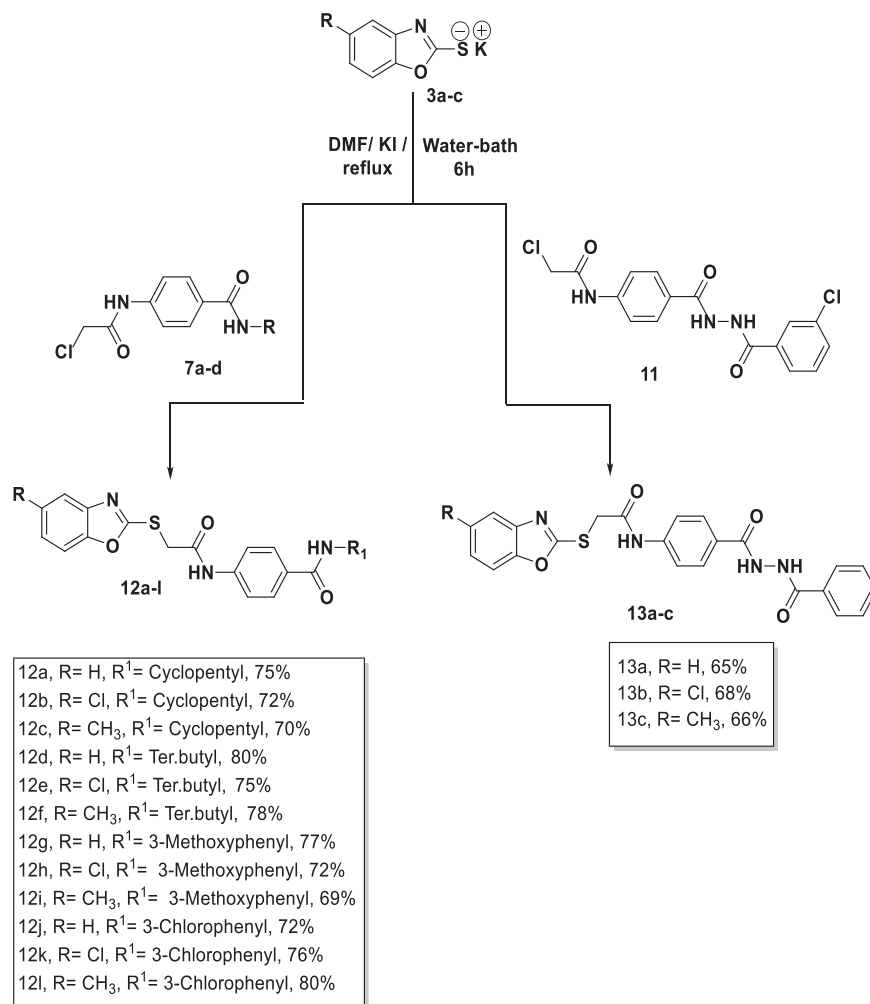
2.2.5. Cell cycle analysis

Compound **12l,** achieved notable cytotoxic and VEGFR-2 inhibitory potencies was further studied mechanistically for cell cycle progression and induction of apoptosis in HepG2 cells. Cell cycle process was analysed after exposure of HepG2 cells to **12l** with a concentration of 10.50 μM for 24 h. Flow cytometry data revealed that the percentage of cells arrested at Pre-G1 phase decreased from 0.93% (in control cells) to 0.79% (in **12l**) treated cells. Additionally, a marked decrease in cell population was observed at the G1 phase (28.34%) comparing to control cells (51.07%). For the S phase compound **12l** induced a significant increase in the cell population (38.68%) comparing to control cells (27.22%). Finally, compound **12l** exhibited significant increase in the cell population (32.10%) at the G2/M phase, comparing to the control cells (20.78%). Such outputs verify that compound **12l** arrested the HepG2 cancer cell's growth mainly at the Pre-G1 and G1 phases (Table 4 and Figure 4).

2.2.6. Apoptosis analysis

The most potent anticancer agent **12l** was selected for the assessment of apoptosis in HepG2 cells using Annexin V/propidium iodide (PI) double staining assay method. In this method, HepG2 cells were incubated with compound **12l** at the IC_{50} concentration (10.50 μM) for 24 h. The results revealed that compounds **12l** could induce apoptosis more than the untreated control cells by a ratio of 35.13%. In details, 32.45 and 2.86% for early and late apoptotic phases, respectively compared to control, (6.56%,5.34%,1.22%, respectively) (Figure 5 and Table 5).

12a, R= H, R^1= Cyclopentyl, 75%
12b, R= Cl, R^1= Cyclopentyl, 72%
12c, R= CH$_3$, R^1= Cyclopentyl, 70%
12d, R= H, R^1= Ter.butyl, 80%
12e, R= Cl, R^1= Ter.butyl, 75%
12f, R= CH$_3$, R^1= Ter.butyl, 78%
12g, R= H, R^1= 3-Methoxyphenyl, 77%
12h, R= Cl, R^1= 3-Methoxyphenyl, 72%
12i, R= CH$_3$, R^1= 3-Methoxyphenyl, 69%
12j, R= H, R^1= 3-Chlorophenyl, 72%
12k, R= Cl, R^1= 3-Chlorophenyl, 76%
12l, R= CH$_3$, R^1= 3-Chlorophenyl, 80%

13a, R= H, 65%
13b, R= Cl, 68%
13c, R= CH$_3$, 66%

Scheme 3. Synthesis of the final compounds **12a-l** and **13a-c**.

2.2.7. Evaluation of BAX and bcl-2 expressions

Compound **12l** was subjected to further cellular mechanistic study. The cellular levels of BAX and Bcl-2 were measured using the western blot technique after compound **12l** was applied to HepG2 cells for 24 h. The results indicated that compound **12l** increased the concentration of the pro-apoptotic factor BAX by 3.40-fold while decreasing the concentration of the anti-apoptotic protein Bcl-2 by 2.12-fold. Furthermore, a significant increase in the BAX/Bcl-2 ratio by 6.83-fold was observed. The obtained findings indicated that compound **12l** was effective in the apoptosis cascade and may encourage the apoptotic pathway (Table 6 and Figure 6).

2.2.8. Caspase 3 assay

Caspase-3 has a key role in apoptosis initiation and execution[26,27]. The western blot technique was used to investigate the effect of compound **12l,** the most promising member, on the caspase-3 level. HepG2 cells were treated with **12l** (10.50 μM) for 24 h. Comparing control HepG2 cells, compound **12l** caused a significant increase in the cellular levels of caspase-3 (2.98-fold) as presented in Table 6 and Figure 6.

2.3. In silico studies

2.31.1. Docking study

To understand the pattern by which the synthesised compounds bound to the active site[28,29], all compounds were subjected to a docking study into the VEGFR-2 ATP binding site (PDB: 4ASD, resolution: 2.03 Å). The native co-crystallized inhibitor, sorafenib, was adopted as a reference in the present work. Following the preparation of the downloaded protein, a validation step was carried out in which the native inhibitor, sorafenib, was re-docked against the catalytic VEGFR-2 site. Results of the previous step successfully reproduced an identical binding pattern to that of the co-crystallized ligand with an RMSD value of 0.71 Å Figure 7. Thus, the later findings supported the validity of the suggested docking protocol.

Observation of the kinds of interaction between sorafenib and the VEGFR-2 catalytic site revealed that it could form two interaction types (Figure 8). The 1st type is an H-bonding interaction, as sorafenib formed two H-bonds with a critical amino acid (Cys919) in the hinge region in addition to three H-bonds with the DFG motif amino acids (Asp1046 and Glu885). The 2nd interaction type included different π interactions between sorafenib and the hydrophobic amino acids among the active pocket.
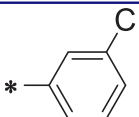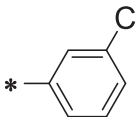
Docking conformations of the synthesised derivatives revealed that they were stacked onto the VEGFR-2 catalytic site in a way similar to that of the original ligand. However, the predicted docking pose of compound **12l** showed that its benzoxazole fragment was linked to the hinge region Cys919 amino acid via a strong H-bond. Additionally, compound **12l** interacted by an H-bond with Glu885 and two H-bonds with Asp1046 in the DFG motif (Figure 9). The later binding pattern gave a reasonable explanation for **12l** of being the most active biologically among the tested

Table 1. *In vitro* anti-proliferative effects of the obtained compounds against HepG2 and MCF-7 cell lines.
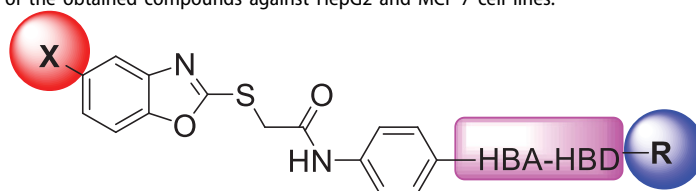
Comp. No.	X	HBA-HBD	R	In vitro IC$_{50}$ (μM) [a]	
				HepG2	MCF-7
12a	H	-NH-CO-		38.83 ± 3.2	33.27 ± 2.9
12b	Cl	-NH-CO-		64.16 ± 6.1	77.03 ± 7.3
12c	CH$_3$	-NH-CO-		74.30 ± 6.8	36.72 ± 3.3
12d	H	-NH-CO-		23.61 ± 2.1	44.09 ± 3.8
12e	Cl	-NH-CO-		71.59 ± 6.7	62.29 ± 5.8
12f	CH$_3$	-NH-CO-		36.96 ± 3.4	22.54 ± 1.8
12g	H	-NH-CO-		36.67 ± 2.9	53.01 ± 5.1
12h	Cl	-NH-CO-		102.10 ± 8.5	85.62 ± 8.2
12i	CH$_3$	-NH-CO-		27.30 ± 2.2	27.99 ± 2.1
12j	H	-NH-CO-		50.92 ± 4.6	33.61 ± 2.8
12k	Cl	-NH-CO-		28.36 ± 2.5	86.62 ± 7.8
12l	CH$_3$	-NH-CO-		**10.50** ± 0.8	**15.21** ± 1.1
13a	H	-CO -NH-NH-CO-		25.47 ± 2.1	32.47 ± 2.9
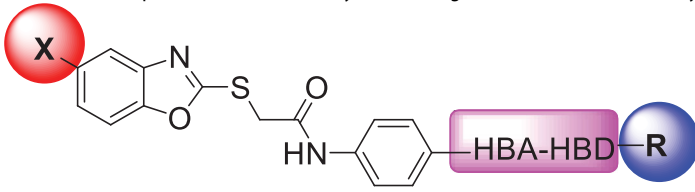
(continued)
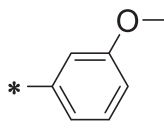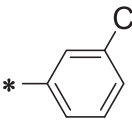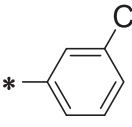
Table 1. Continued.

Comp. No.	X	HBA-HBD	R	In vitro IC$_{50}$ (µM) [a]	
				HepG2	MCF-7
13b	Cl	-CO -NH-NH-CO-	(3-chlorophenyl)	42.06 ± 3.8	26.31 ± 2.2
13c	CH$_3$	-CO -NH-NH-CO-	(3-chlorophenyl)	24.25 ± 2.1	53.13 ± 3.7
Sorafenib	-	-	-	5.57 ± 0.4	6.46 ± 0.3

[a]Data are presented as mean of the IC$_{50}$ values from three different experiments.

Table 2. IC$_{50}$ values of the tested compounds on the inhibitory activities against VEGFR-2 Kinases Assay.

Comp. No.	X	HBA-HBD	R	VEGFR-2, IC$_{50}$ (nM)
12d	H	-NH-CO-	(tert-butyl)	194.60
12f	CH$_3$	-NH-CO-	(tert-butyl)	264.90
12i	CH$_3$	-NH-CO-	(3-methoxyphenyl)	155.00
12l	CH$_3$	-NH-CO-	(3-chlorophenyl)	97.38
13a	H	-CO -NH-NH-CO-	(3-chlorophenyl)	267.80
Sorafenib	-	-	-	48.16

compounds. A superimposition poses of **12l** and the native ligand, sorafenib, provided additional evidence to the obtained results. As presented in Figure 10, compound **12l** and sorafenib generally overlapped well and had the same 3-D orientation. Niceties revealed that the pharmacophoric moieties of sorafenib represented by N-methylpicolinamide, phenoxy, urea, and 4-chloro-3-(trifluoromethyl)phenyl) moieties had the same orientation with the 5-methylbenzo[d]oxazol, N-phenylacetamide, amide, and 3-chlorophenyl moieties, respectively of compound **12l**.

2.3.2. Pharmacokinetic profiling study
In the current study, an in silico computational study of the tested candidates was conducted following the directions of Veber's and Lipinski's rule of five[30,31].

The obtained findings presented in Table 7 showed that all tested compounds showed no contravention of Lipinski's and Veber's Rules and hence display a drug-like molecular nature. In detail, the LogP, molecular weight, number of H-bond donors, and number of H-bond acceptors of these fifteen compounds are within the accepted values of less than 5, 500, 5, and 10, respectively. Moreover, the number of rateable bonds and TPSA of such compounds are within the acceptable values of less than 10 and 140 Å^2, respectively.

2.3.3. Swissadme study
To compute the physicochemical properties and the drug likeness properties of the most potent compounds **12d, 12i,** and **12 l**, SwissADME online web tool was applied. The obtained results
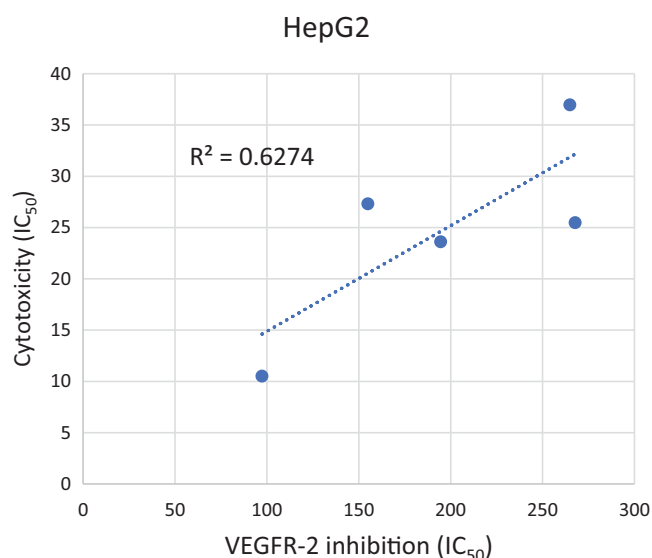
HepG2

Figure 3. Correlation graph study.

Table 3. IC$_{50}$ results of **12d**, **12i**, and **12l** against WI-38 cell line.

Compound	WI-38, IC$_{50}$ (µM)
12d	99.41
12i	76.78
12l	37.79
Sorafenib	22.10

Table 4. Supressing potentialities of **12l** on the cell cycle of HepG2 cells after 24 h treatment.

Sample	Cell cycle distribution (%)[a]			
	%Sub-G1	%G1	%S	% G2/M
HepG2	0.93 ± 0.02	51.07 ± 1.03	27.22 ± 1.24	20.78 ± 0.23
Compound 12 l /HepG2	0.79 ± 0.25	28.43 ± 0.37**	38.68 ± 1.81*	32.10 ± 181**

[a]Values are given as mean ± SEM of two independent experiments and *$p < 0.05$; **$p < 0.01$.

predicted that the physicochemical properties of the three candidates were in acceptable ranges, hence they may have good oral bioavailability. Also, they are expected to hve undesirable effects on CNS as they cannot pass BBB (Table 8). Furthermore, SwissADME revealed that compounds **12d, 12i,** and **12l** fulfilled Lipinskìs, Veber's, and Ghose's rules predicting that these compounds have promising drug-likeness profiles (Table 7). Moreover, the radar charts which involved the calculation of six parameters including lipophilicity, polarity, flexibility, size, saturation, and solubility showed that compounds **15 b** and **17 b** (represented by red lines and integrated into the pink area) are almost predicting acceptable oral bioavailability (Table 9).

3. Conclusion

In the present study, fifteen benzoxazole derivatives were designed, synthesised as potential anticancer and VEGFR-2 inhibitors. The anticancer potentialities of the obtained derivatives were estimated against HepG2, and MCF-7 cell lines cell lines. Five compounds **12d** (IC$_{50}$ = 23.61 & 44.09 µM), **12f** (IC$_{50}$ = 36.96 & 22.54 µM), **12i** (IC$_{50}$ = 27.30 & 27.99 µM), compounds **12d** (IC$_{50}$ = 23.61 & 44.09 µM), **12f** (IC$_{50}$ = 36.96 & 22.54 µM), **12i** (IC$_{50}$ = 27.30

& 27.99 µM), and **13a** (IC$_{50}$ = 11.4 & 14.2 µM) displayed noticeable anticancer activities against HepG2 and MCF-7, respectively. Moreover, VEGFR-2 kinase inhibition assay results revealed that compound **12l** showed the most potent inhibitory activity against VEGFR-2, comparing the reference drug, sorafenib. Owing to its notable high antiproliferative and VEGFR-2 inhibitory activities, derivative **12l** was selected for further evaluation to understand its mechanistic studies. Cell cycle analysis indicated that **12l** could arrest the malignant HepG2cells at the Pre-G1 and G1 phases and induced apoptosis by 35.13%, compared to 6.56% in the control cells. Additionally, compound **12l** exhibited significant potential to increase caspase 3 (BAX and BAX/Bcl-2 ratio with (2.98, 3.40- and 6.83 folds, respectively). Similarly, it decreased Bcl-2 (2.12-fold) comparing the untreated cells. Molecular docking studies were accomplished for all the target derivatives. Docking findings supported biological activity results where the most potent VEGFR-2 inhibitor was able to incorporate the tyrosine kinase domain of VEGFR-2 in a fashion comparable to that of the well-known VEGFR-2 inhibitor, sorafenib.

4. Experimental

4.1. Chemistry

In Supplementary data, all apparatus used in the analysis of produced chemicals were elucidated. Compounds **2a-c**, **3a-c**, **6**, **7a-c**, **9**, **10**, and **11** were synthesised using procedures that have previously been reported[32]. The ^{1}H/^{13}C NMR analyses were carried out at 400 and 100 MHz, respectively in DMSO-d$_6$ as a solvent. The chemical shifts were presented as ppm. The infra-red investigations were carried out using KBr disc and the results were presented as cm^{-1}. The colours and meting points of the final compounds **12a-l** and **13a-c** were presented in Table 10.

4.1.1. General procedure for preparation of the target compounds 12a-l

In 10 ml DMF containing 0.001 mol KI, 0.001 mol of **3a-c** and 0.001 mol of the appropriate benzamide derivatives **7a-d** were mixed and heated under reflux for 6 h. The reaction content was then poured on crushed ice. The collected crystals were filtered and crystalised from methanol to afford **12a-l**.

4.1.1.1. 4–(2-(Benzo[d]oxazol-2-ylthio)acetamido)-N-cyclopentyl-benzamide 12a. IR: 3495, 3383 (NH), 3054 (CH aromatic), 2951 (CH aliphatic), 1661, 1623 (C=O); ^{1}H NMR: 10.69 (s, 1H), 8.20 (d, J = 7.3 Hz, 1H), 7.85 (d, J = 8.4 Hz, 2H), 7.75–7.59 (m, 4H), 7.40–7.28 (m, J = 6.7, 5.4 Hz, 2H), 4.44 (s, 2H), 4.23 (h, J = 7.0 Hz, 1H), 1.89 (m, 2H), 1.79–1.64 (m, 2H), 1.59–1.50 (m, 4H); ^{13}C NMR: 165.81, 165.79, 164.32, 151.82, 141.68, 141.52, 128.74, 125.15, 124.83, 118.71, 110.69, 51.38, 37.26, 32.62, 24.10; MS (m/z) for C$_{21}$H$_{21}$N$_3$O$_3$S (395.48): 395.50 (M$^+$, 100%).

4.1.1.2. 4–(2-((5-Chlorobenzo[d]oxazol-2-yl)thio)acetamido)-N-cyclopentylbenzamide 12b. IR: 3414, 3272 (NH), 3064 (CH aromatic), 2938 (CH aliphatic), 1656 (C=O); ^{1}H NMR: 10.68 (s, 1H), 8.20 (d, J = 7.3 Hz, 1H), 7.85 (d, J = 8.3 Hz, 2H), 7.76–7.63 (m, 4H), 7.37 (dd, J = 8.7, 2.1 Hz, 1H), 4.45 (s, 2H), 4.22 (h, J = 7.2 Hz, 1H), 1.89 (m, 2H), 1.69 (m, 2H), 1.53 (m, 4H); ^{13}C NMR: 166.37, 165.93, 165.66, 150.58, 142.91, 141.44, 130.14, 129.48, 128.72, 124.80, 118.78, 118.46, 111.99, 51.40, 37.22, 32.57, 24.07.

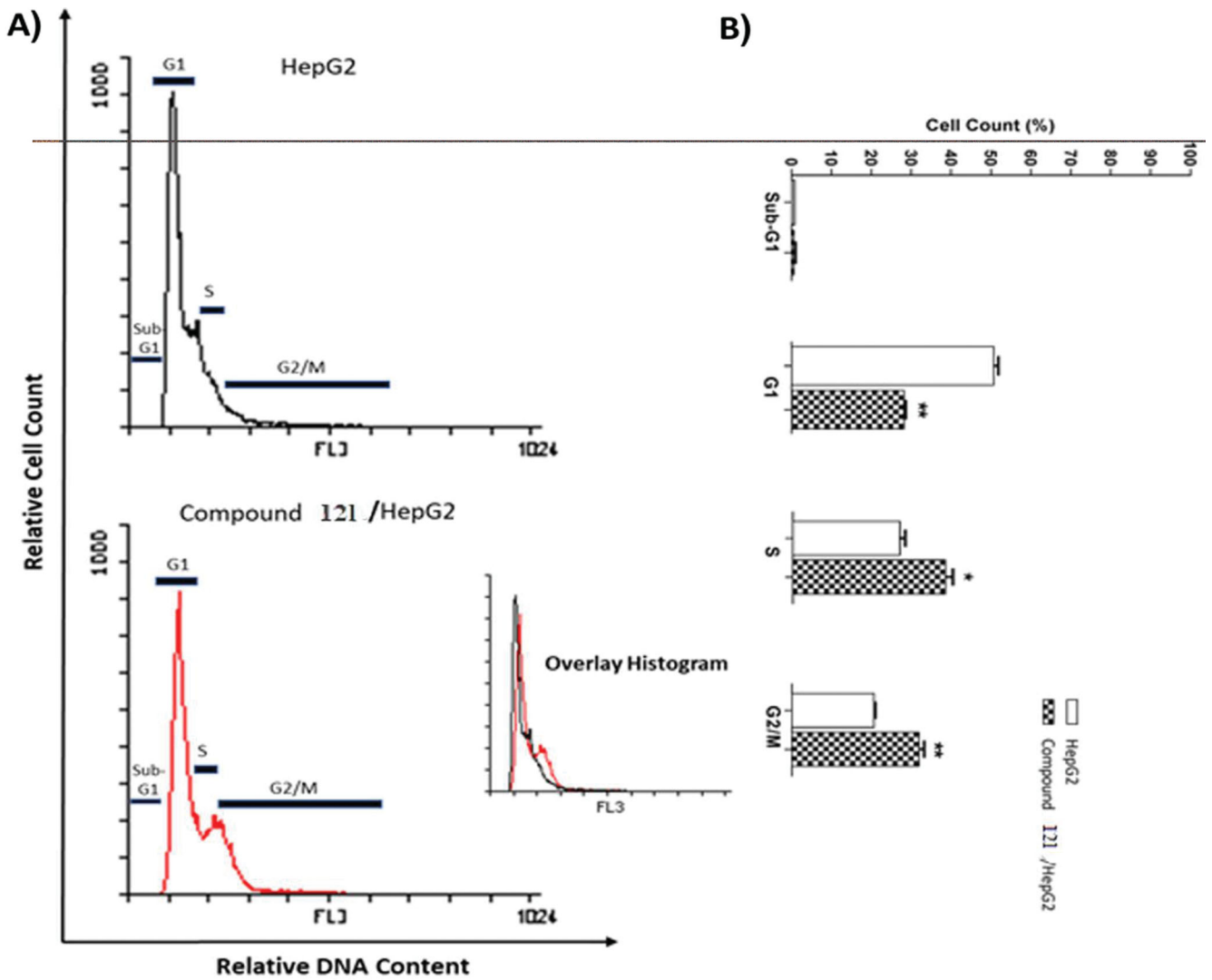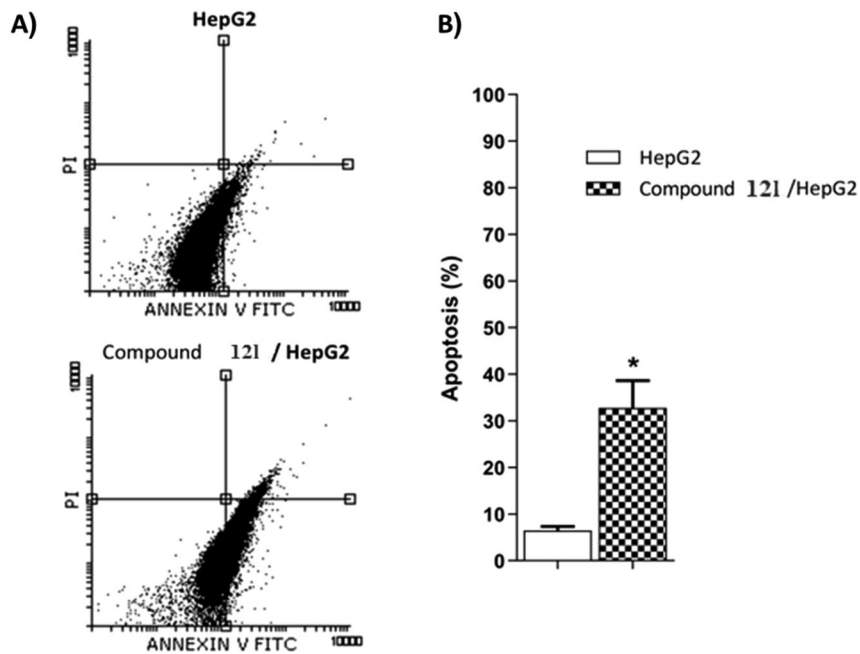**Figure 4.** Flow cytometry analysis of HepG2 cell cycle after the treatment of compound **12l**.

Figure 5. Flow cytometry analysis of compound **12l** apoptotic induction against HepG2 cells.

4.1.1.3. N-Cyclopentyl-4–(2-((5-methylbenzo[d]oxazol-2-yl)thio)acetamido)benzamide 12c. IR: 3273 (NH), 3041 (CH aromatic), 2945 (CH aliphatic), 1657, 1618 (C=O); ^{1}H NMR: 10.68 (s, 1H), 8.20 (d, $J = 7.3$ Hz, 1H), 7.86 (d, $J = 8.4$ Hz, 2H), 7.67 (d, $J = 8.4$ Hz, 2H), 7.51 (d, $J = 8.3$ Hz, 1H), 7.42 (s, 1H), 7.16–7.09 (m, 1H), 4.42 (s, 2H), 4.23 (h, $J = 7.0$ Hz, 1H), 2.39 (s, 3H), 1.88 (m, 2H), 1.76–1.64 (m, 2H), 1.62–1.46 (m, 4H); ^{13}C NMR: 165.81, 164.17, 150.07, 141.70, 134.54, 130.16, 129.46, 125.60, 118.66, 110.04, 51.38, 37.26, 32.62, 24.10, 21.38; MS (m/z) for $C_{22}H_{23}N_3O_3S$ (409.50): 409.48 (M$^+$, 100%).

4.1.1.4. 4–(2-(Benzo[d]oxazol-2-ylthio)acetamido)-N-(tert-butyl)benzamide 12d. IR: 3377, 3272 (NH), 3038 (CH aromatic), 2971 (CH aliphatic), 1613 (C=O); ^{1}H NMR: 10.68 (s, 1H), 7.81 (d, $J = 8.3$ Hz, 2H),

Table 5. Apoptotic potentialities compound **12l** against HepG2 cells after 24 h treatment.

| Sample | Viable a (Left Bottom) | Apoptosis a | | Necrosis a (Left Top) |
		Early (Right Bottom)	Late (Right Top)	
HepG2	92.96 ± 0.55	5.34 ± 0.01	1.22 ± 0.77	0.48 ± 0.27
12l / HepG2	64.55 ± 3.43	$32.45 \pm 3.13^*$	2.86 ± 0.21	0.14 ± 0.06

^{a}Values are given as mean $\pm$ SEM of two independent experiments. $^*p < 0.05$.

Table 6. Effect of compound **12l** on the levels of BAX, Bcl-2, and Caspase-3 proteins expression in HepG2 cells treated for 24 h.

| Sample | Protein expression (normalized to β-actin) a | | | |
	BAX	Bcl-2	BAX/Bcl-2 ratio	Caspase-3
HepG2	1.00 ± 0.08	1.00 ± 0.32	1.00 ± 0.25	1.00 ± 0.06
12l	$3.40 \pm 0.15^{**}$	0.47 ± 0.05	$6.83 \pm 0.96^*$	$2.98 \pm 0.13^{**}$

^{a}Values are given as mean $\pm$ SEM of two independent experiments. $^*p < 0.05$, $^{**}p < 0.01$.

7.75 − 7.57 (m, 5H), 7.39–7.27 (m, 2H), 4.44 (s, 2H), 1.38 (s, 9H); MS (m/z) for $C_{20}H_{21}N_3O_3S$ (383.47): 383.28 (M$^+$, 100%).

4.1.1.5. N-(Tert-butyl)-4–(2-((5-chlorobenzo[d]oxazol-2-yl)thio)acetamido)benzamide 12e. IR: 3412, 3277 (NH), 3072 (CH aromatic), 2951 (CH aliphatic), 1655, 1604 (C=O); ^{1}H NMR: 10.70 (s, 1H), 7.81 (d, $J = 8.5$ Hz, 2H), 7.73 (d, $J = 2.1$ Hz, 1H), 7.71–7.62 (m, 4H), 7.36 (dd, $J = 8.7$, 2.2 Hz, 1H), 4.45 (s, 2H), 1.38 (s, 9H); ^{13}C NMR: 166.42, 166.08, 165.57, 150.60, 142.96, 141.32, 131.22, 129.46, 128.77, 124.74, 118.61, 118.48, 111.95, 51.17, 37.41, 29.10; MS (m/z) for $C_{20}H_{20}ClN_3O_3S$ (417.91): 417.36 (M$^+$, 100%).

4.1.1.6. N-(Tert-butyl)-4–(2-((5-methylbenzo[d]oxazol-2-yl)thio)acetamido)benzamide 12f. IR: 3383, 3286 (NH), 3072 (CH aromatic), 2965 (CH aliphatic), 1709, 1626 (C=O); ^{1}H NMR: 10.66 (s, 1H), 7.88–7.73 (m, 2H), 7.72–7.58 (m, 3H), 7.53 (d, $J = 8.3$ Hz, 1H), 7.47–7.36 (m, 1H), 7.14 (dd, $J = 8.4$, 1.7 Hz, 1H), 4.41 (s, 2H), 2.40 (s, 3H), 1.38 (s, 9H); MS (m/z) for $C_{21}H_{23}N_3O_3S$ (397.49): 397.43 (M$^+$, 100%).

4.1.1.7. 4–(2-(Benzo[d]oxazol-2-ylthio)acetamido)-N-(3-methoxyphenyl)benzamide 12 g. IR: 3262 (NH), 3033 (CH aromatic), 2927 (CH aliphatic), 1647 (C=O); ^{1}H NMR: 10.83 (s, 1H), 10.17 (s, 1H), 8.00 (d, $J = 8.3$ Hz, 2H), 7.78 (d, $J = 8.3$ Hz, 2H), 7.66 (p, $J = 5.8$ Hz, 2H), 7.51 (t, $J = 2.3$ Hz, 1H), 7.41 (d, $J = 8.1$ Hz, 1H), 7.38–7.27 (m, 2H), 7.25 (d, $J = 8.1$ Hz, 1H), 6.68 (dd, $J = 8.3$, 2.5 Hz, 1H), 4.48 (s, 2H), 3.77 (s, 3H); ^{13}C NMR: 165.99, 165.32, 164.17, 159.89, 150.09, 141.88, 140.93, 134.58, 129.82, 129.23, 125.65, 118.86, 118.67, 113.01, 110.10, 106.48, 55.47, 21.40; MS (m/z) for $C_{23}H_{19}N_3O_4S$ (433.48): 433.34 (M$^+$, 100%).

4.1.1.8. 4–(2-((5-Chlorobenzo[d]oxazol-2-yl)thio)acetamido)-N-(3-methoxyphenyl)benzamide 12 h. IR: 3412, 3259 (NH), 3065 (CH
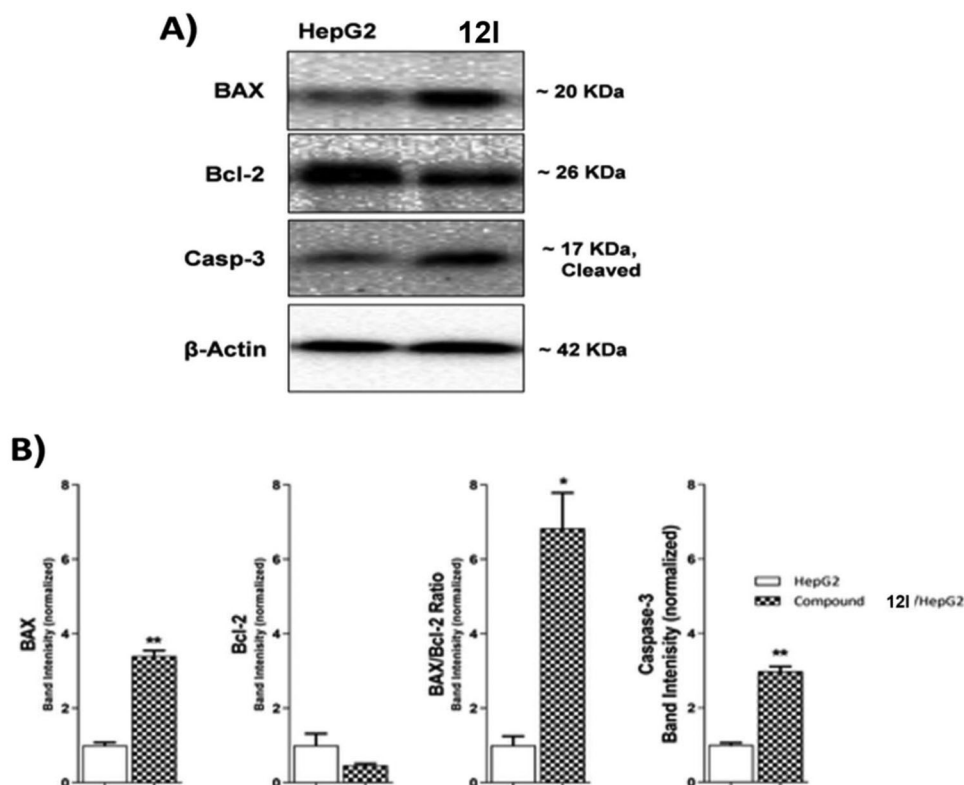

Figure 6. The immunoblotting of effect of compound **12l** against BAX, Bcl-2, and Caspase-3.
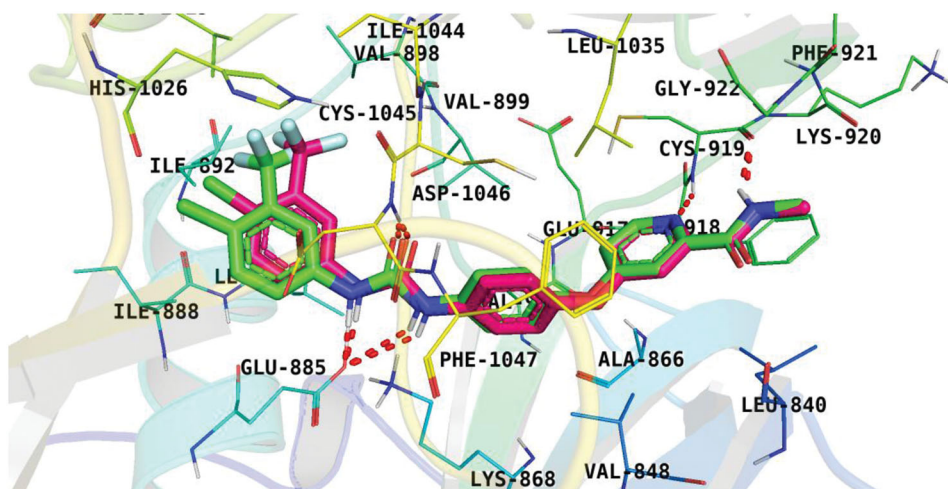
Figure 7. Results of the re-docking step into the VEGFR-2 catalytic site; native ligand (green) and the obtained pose (red).
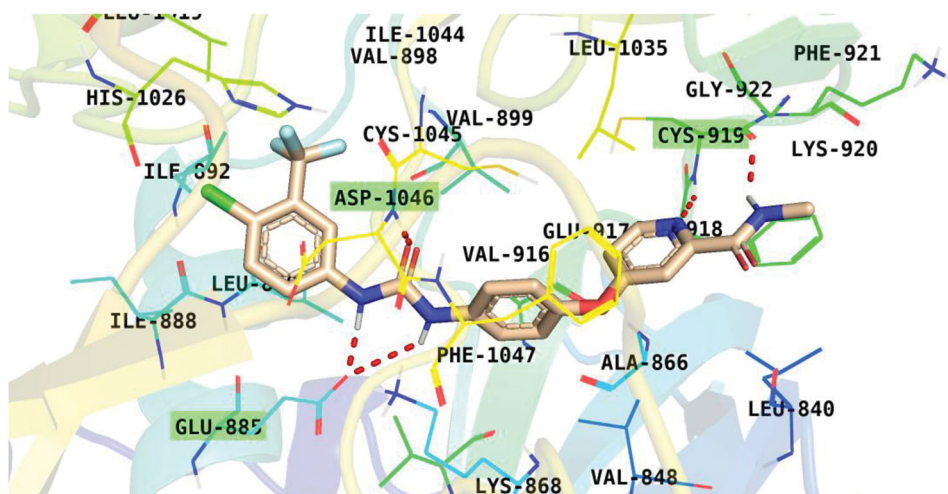

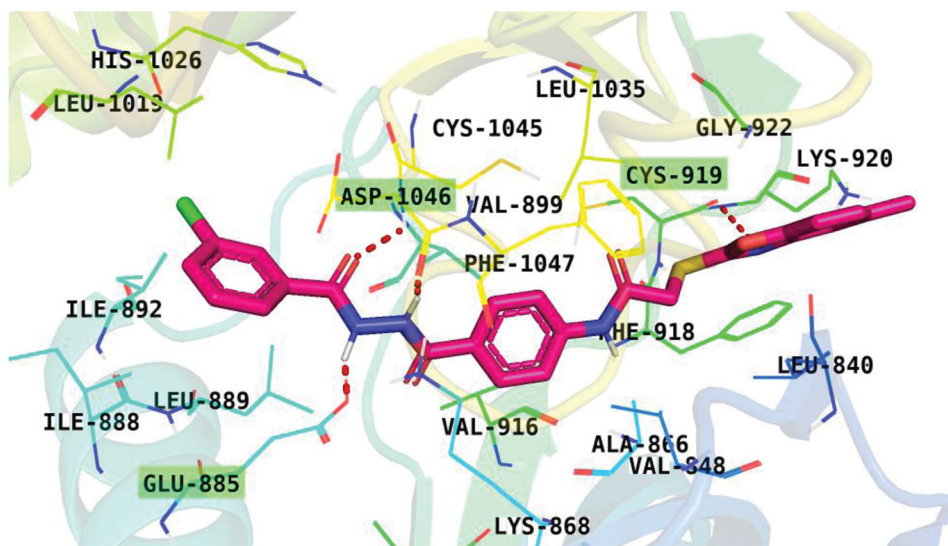**Figure 8.** Sorafenib binding interactions with VEGFR-2 catalytic site.

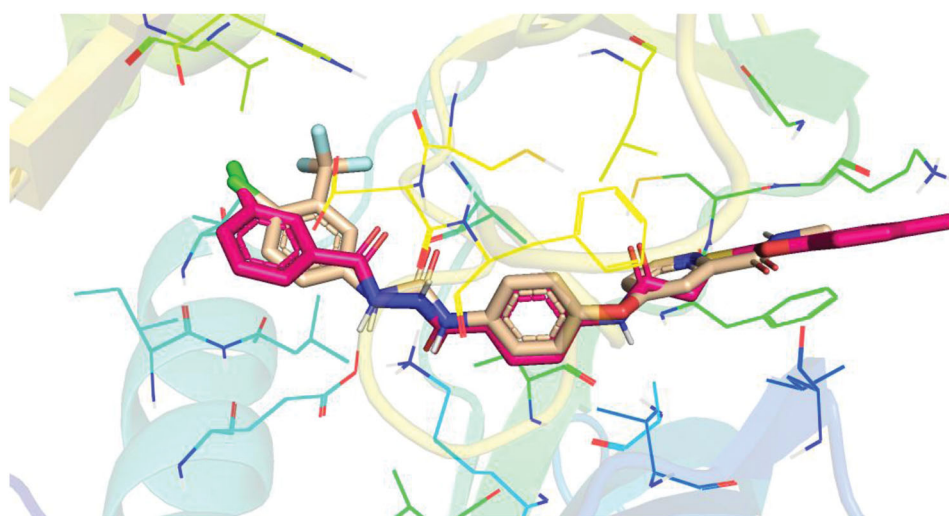**Figure 9.** Binding pose of **12l** with the active site of VEGFR-2.

Figure 10. Superimposition of **12l** (red) and sorafenib (wheat) inside the VEGFR-2 catalytic site.

Table 7. Physicochemical properties of the tested compounds passed Lipinski and Veber Rules

	Lipinski Rules				Veber Rules	
Comp.	Num HD	Num HA	M Wt	AlogP	Num Rotatable Bonds	TPSA
12a	2	4	395.475	3.685	6	109.53
12b	2	4	429.92	4.35	6	109.53
12c	2	4	409.501	4.171	6	109.53
12d	2	4	383.464	3.214	6	109.53
12e	2	4	417.909	3.879	6	109.53
12f	2	4	397.491	3.701	6	109.53
12g	2	5	433.48	3.843	7	118.76
12h	2	5	467.925	4.508	7	118.76
12i	2	5	447.506	4.33	7	118.76
12j	2	4	437.899	4.524	6	109.53
12k	2	4	472.344	5.189	6	109.53
12l	2	4	451.925	5.01	6	109.53
13a	3	5	446.478	3.117	7	138.63
13b	3	5	480.923	3.781	7	138.63
13c	3	5	460.505	3.603	7	138.63

Table 8. ADME profile of compounds **12d, 12i,** and **12l**

Parameter	12d	12i	12l
Physicochemical properties			
Molecular weight	383.46	447.51	451.93
Num. heavy atoms	27	32	31
Num. H-bond acceptors	4	5	4
Num. H-bond donors	2	2	2
Molar Refractivity	107.02	125.24	123.75
TPSA	109.53 Å^2	118.76 Å^2	109.53 Å^2
Consensus Log $P_{o/w}$	3.34	3.98	4.48
Log S (ESOL)	Moderately soluble	Moderately soluble	Moderately soluble
Drug likeness			
Lipinski violations	Yes; 0 violation	Yes; 0 violation	Yes; 0 violation
Ghose violations	Yes	Yes	Yes
Veber violations	Yes	Yes	Yes
Bioavailability Score	0.55	0.55	0.55
Pharmacokinetics			
GI absorption	High	Low	Low
BBB permeant	No	No	No
CYP1A2 inhibitor	Yes	Yes	Yes
CYP2C19 inhibitor	Yes	Yes	Yes
CYP2C9 inhibitor	Yes	Yes	Yes
CYP2D6 inhibitor	Yes	Yes	Yes
CYP3A4 inhibitor	Yes	Yes	Yes

aromatic), 2991, 2933 (CH aliphatic), 1656 (C=O); ^{1}H NMR: 10.80 (s, 1H), 10.15 (s, 1H), 7.99 (d, J = 8.3 Hz, 2H), 7.86–7.70 (m, 3H), 7.67 (d, J = 8.7 Hz, 1H), 7.50 (s, 1H), 7.38 (dd, J = 18.8, 8.4 Hz, 2H), 7.25 (t, J = 8.2 Hz, 1H), 6.67 (d, J = 8.3 Hz, 1H), 4.48 (s, 2H), 3.76 (s, 3H); ^{13}C NMR: 166.42, 166.08, 165.57, 150.60, 142.96, 141.32, 131.22, 129.46, 128.77, 124.74, 118.61, 118.48, 111.95, 51.17, 29.10; MS (m/z) for $C_{23}H_{18}ClN_3O_4S$ (467.92): 467.17 (M$^+$, 40%), 345.36 (100%).

4.1.1.9. N-(3-Methoxyphenyl)-4–(2-((5-methylbenzo[d]oxazol-2-yl)thio)acetamido)benzamide 12i. IR: 3385, 3282 (NH), 3073 (CH aromatic), 2931 (CH aliphatic), 1688, 1648 (C=O); ^{1}H NMR: 10.79 (s, 1H), 10.15 (s, 1H), 7.98 (d, J = 8.4 Hz, 2H), 7.76 (d, J = 8.4 Hz, 2H), 7.56–7.46 (m, 2H), 7.44 (d, J = 1.7 Hz, 1H), 7.39 (dd, J = 8.1, 1.9 Hz, 1H), 7.25 (t, J = 8.1 Hz, 1H), 7.14 (dd, J = 8.4, 1.7 Hz, 1H), 6.68 (dd, J = 8.2, 2.5 Hz, 1H), 4.45 (s, 2H), 3.76 (s, 3H), 2.40 (s, 3H); ^{13}C NMR: 165.99, 165.32, 164.17, 159.89, 150.09, 142.14, 141.88, 140.93, 134.58, 130.11, 129.82, 129.23, 125.65, 118.86, 118.67, 113.01, 110.10, 109.50, 106.48, 55.47, 37.27, 21.40; MS (m/z) for $C_{24}H_{21}N_3O_4S$ (447.51): 447.32 (M$^+$, 100%).

4.1.1.10. 4–(2-(Benzo[d]oxazol-2-ylthio)acetamido)-N-(3-chlorophe-nyl)benzamide 12j. IR: 3384, 3276 (NH), 3066 (CH aromatic), 2981 (CH aliphatic), 1657 (C=O); ^{1}H NMR: 10.80 (s, 1H), 10.33 (s, 1H),

8.03–7.93 (m, 3H), 7.82–7.63 (m, 5H), 7.43–7.31 (m, 3H), 7.17 (td, J = 9.2, 8.1, 2.2 Hz, 1H), 4.34 (d, J = 96.7 Hz, 2H); ^{13}C NMR: 166.00, 165.55, 164.30, 151.83, 142.34, 141.68, 141.23, 133.41, 130.75, 129.34, 124.85, 120.16, 118.92, 118.74, 110.72, 37.29. MS (m/z) for $C_{22}H_{16}ClN_3O_3S$ (437.90): 437.33 (M$^+$, 10%), 120.20 (100%).

4.1.1.11. 4–(2-((5-Chlorobenzo[d]oxazol-2-yl)thio)acetamido)-N-(3-chlorophenyl)benzamide 12k. IR: 3379, 3265 (NH), 3093 (CH aromatic), 2980 (CH aliphatic), 1644 (C=O); ^{1}H NMR: 10.82 (s, 1H), 10.33 (s, 1H), 8.10–7.91 (m, 3H), 7.85–7.59 (m, 5H), 7.42–7.32 (m, 2H), 7.14 (dd, J = 8.0, 2.1 Hz, 1H), 4.48 (s, 2H); ^{13}C NMR: 166.39, 165.79, 165.52, 150.61, 142.96, 142.31, 141.24, 133.41, 130.70, 129.34, 124.73, 120.15, 118.91, 118.49, 111.94, 37.46; MS (m/z) for $C_{22}H_{15}Cl_2N_3O_3S$ (472.34): 472.70 (M$^{+,}$ 30%) 345.20 (100%).

4.1.1.12. N-(3-Chlorophenyl)-4–(2-((5-methylbenzo[d]oxazol-2-yl)thio)acetamido)benzamide 12l. IR: 3384, 3181 (NH), 3034 (CH aromatic), 2970 (CH aliphatic), 1651 (C=O); ^{1}H NMR 10.83 (s, 1H), 10.35 (s, 1H), 8.26–6.84 (m, 11H), 4.45 (s, 2H), 2.44 (s, 3H); MS (m/z) for $C_{23}H_{18}ClN_3O_3S$ (451.93): 451.30 (M$^+$, 100%).

Table 9. Radar charts for prediction of oral bioavailability profile of compounds **12d**, **12i**, and **12l**

Compounds	12d	12i	12l
Radar images			
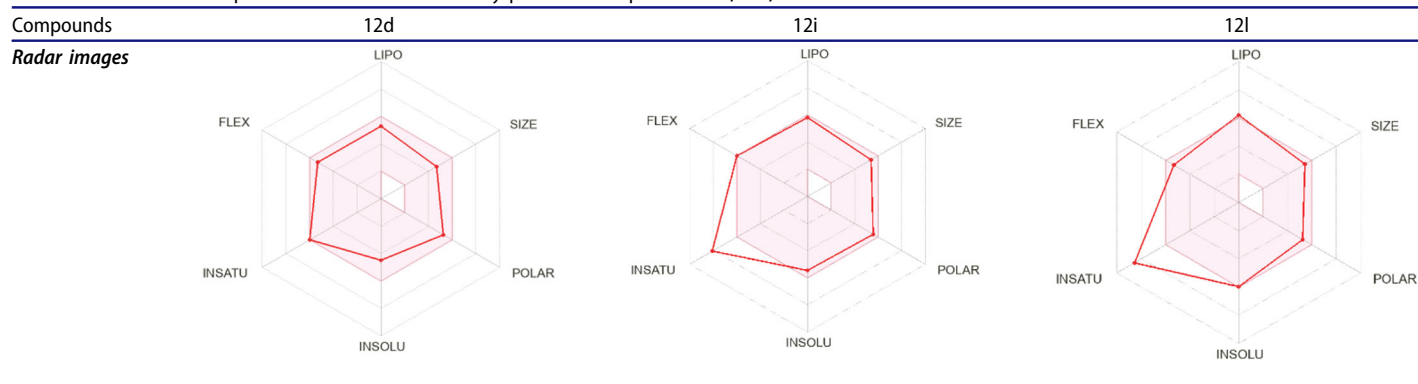
Table 10. Colours, yields, and meting points of the target compounds

Compounds	Color	Meting points (°C)
12a	White crystals	230–232
12b	White crystals	240–242
12c	White crystals	235–237
12d	White crystals	211–215
12e	White crystals	233–235
12f	White crystals	222–224
12g	White crystals	252–254
12h	White crystals	244–246
12i	White crystals	255–257
12j	White crystals	240–242
12k	White crystals	220–222
12l	White crystals	266–268
13a	White crystals	223–225
13b	White crystals	211–213
13c	White crystals	235–237

4.1.2. General procedure for preparation of the target compounds 13a-c

In 10 ml DMF containing 0.001 mol KI, 0.001 mol of **3a-c** and 0.001 mol of N-(4–(2-benzoylhydrazine-1-carbonyl)phenyl)-2-chloroacetamide **11**, were mixed well and refluxed for 6 h. The reaction content was then poured on crushed ice. The collected crystals were filtered and crystalised from methanol to afford **13a-c**.

4.1.2.1. 2-(Benzo[d]oxazol-2-ylthio)-N-(4–(2-(3-chlorobenzoyl)hydrazine-1-carbonyl)phenyl)- acetamide 13a.
IR: 3384, 3279 (NH), 3014 (CH aromatic), 2853 (CH aliphatic), 1660 (C=O); ^{1}H NMR: 10.79 (s, 1H), 10.65 (s, 1H), 10.53 (s, 1H), 8.06–7.85 (m, 4H), 7.76 (d, J = 8.3 Hz, 2H), 7.66 (q, J = 8.7, 8.2 Hz, 3H), 7.58 (t, J = 7.8 Hz, 1H), 7.41–7.29 (m, 2H), 4.47 (s, 2H); MS (m/z) for $C_{23}H_{17}ClN_4O_4S$ (480.92): 480.42 (M$^+$, 10%), 311.23 (100%).

4.1.2.2. 2-((5-Chlorobenzo[d]oxazol-2-yl)thio)-N-(4–(2-(3-chlorobenzoyl)hydrazine-1-carbonyl)- phenyl)acetamide 13 b.
IR: 3279, 3167 (NH), 3017 (CH aromatic), 2855 (CH aliphatic), 1656 (C=O); ^{1}H NMR: 10.79 (s, 1H), 10.65 (s, 1H), 10.53 (s, 1H), 8.10–7.85 (m, 4H), 7.81–7.72 (m, 3H), 7.69 (dd, J = 9.0, 3.4 Hz, 2H), 7.58 (t, J = 7.9 Hz, 1H), 7.37 (dd, J = 8.7, 2.2 Hz, 1H), 4.48 (s, 2H); ^{13}C NMR: 166.39, 165.80, 165.04, 150.61, 142.96, 134.99, 133.87, 131.07, 129.48, 129.08, 127.75, 126.66, 124.76, 119.02, 118.51, 111.97, 37.44; MS (m/z) for $C_{23}H_{16}Cl_2N_4O_4S$ (515.37): 415.76 (M$^+$, 10%), 345.24 (100%).

4.1.2.3. N-(4–(2-(3-Chlorobenzoyl)hydrazine-1-carbonyl)phenyl)-2-((5-methylbenzo[d]oxazol-2-yl)thio)acetamide 13c.
IR: 3279 (NH), 3015 (CH aromatic), 2927 (CH aliphatic), 1657 (C=O); ^{1}H NMR: 10.78 (s, 1H), 10.67 (s, 1H), 10.55 (s, 1H), 8.01–7.89 (m, 4H), 7.78 (d, J = 8.3 Hz, 2H), 7.71–7.64 (m, 1H), 7.58 (t, J = 7.9 Hz, 1H), 7.51 (d, J = 8.3 Hz, 1H), 7.42 (s, 1H), 7.11 (d, J = 8.3 Hz, 1H), 4.46 (s, 2H), 2.39 (s, 3H); ^{13}C NMR: 166.05, 165.76, 165.07, 164.16, 150.10, 142.41, 141.89, 135.00, 134.55, 133.89, 131.05, 129.08, 127.77, 126.66, 125.62, 119.02, 110.05, 37.32, 21.39; MS (m/z) for $C_{24}H_{19}ClN_4O_4S$ (494.95): 494.47 (M$^+$, 10%), 402.37 (100%).

4.2. Biological evaluation

4.2.1. In vitro anti-proliferative activity
MTT assay protocol[32]. This method was applied in accordance with the comprehensive description in Supplementary data.

4.2.2. In vitro VEGFR-2 kinase assay
The assay was applied by ELISA kits in accordance with the comprehensive description in[18,33] as described in Supplementary data.

4.2.3. Flow cytometry analysis for cell cycle
This assay was applied using propidium iodide (PI) staining in accordance with the comprehensive description in Supplementary data[34,35]

4.2.4. Flow cytometry analysis for apoptosis
Apoptotic effect was applied in accordance with the comprehensive description in Supplementary data[36,37]

4.2.5. Western blot analysis
The western blot technique was applied in accordance with the comprehensive description in Supplementary data[38–40]

4.3. In silico studies

4.3.1. Docking studies
Docking studies were applied using MOE 2014[41–43] in accordance with the comprehensive description in were carried out against VEEGFR-2 (PDB ID: 4ASD, resolution: 2.03 Å) as described in Supplementary data.

4.3.2. Pharmacokinetic profiling study
This study was applied using Discover studio 4 in accordance with the comprehensive description in Supplementary data[44].

4.3.3. ADME studies

was used to compute the physicochemical properties and predict the drug likeness properties of the most potent compounds This study was applied using the SwissADME online web tool in accordance with the comprehensive description in Supplementary data[45–47].

ORCID

Hazem A. Mahdy http://orcid.org/0000-0002-6620-241X
Aisha A. Alsfouk http://orcid.org/0000-0003-4497-5013
Mohamed M. Khalifa http://orcid.org/0000-0002-8146-993X
Ibrahim H. Eissa http://orcid.org/0000-0002-6955-2263

References

1. Yang JD, Hainaut P, Gores GJ, et al. A global view of hepatocellular carcinoma: trends, risk, prevention and management. Nat Rev Gastroenterol Hepatol 2019;16:589–604.
2. Paci A, Veal G, Bardin C, et al. Review of therapeutic drug monitoring of anticancer drugs part 1–cytotoxics. Euro J Cancer 2014;50:2010–9.
3. Abdelgawad MA, El-Adl K, El-Hddad SS, et al. Design, molecular docking, synthesis, anticancer and anti-hyperglycemic assessments of thiazolidine-2, 4-diones Bearing Sulfonylthiourea Moieties as Potent VEGFR-2 Inhibitors and PPARγ Agonists. Pharmaceuticals 2022;15:226.
4. Chen H, Kovar J, Sissons S, et al. A cell-based immunocytochemical assay for monitoring kinase signaling pathways and drug efficacy. Anal Biochem 2005;338:136–42.
5. Traxler P, Furet P. Strategies toward the design of novel and selective protein tyrosine kinase inhibitors. Pharmacol Therapeutics 1999;82:195–206.
6. Kang D, Pang X, Lian W, et al. Discovery of VEGFR2 inhibitors by integrating naïve Bayesian classification, molecular docking and drug screening approaches. RSC Adv 2018;8:5286–97.
7. El-Helby A-GA, Sakr H, Ayyad RR, et al. Design, synthesis, molecular modeling, in vivo studies and anticancer activity evaluation of new phthalazine derivatives as potential DNA intercalators and topoisomerase II inhibitors. Bioorg Chem 2020;103:104233.
8. Veeravagu A, Hsu AR, Cai W, et al. Vascular endothelial growth factor and vascular endothelial growth factor receptor inhibitors as anti-angiogenic agents in cancer therapy. Recent Patents Anti Cancer Drug Disc 2007;2:59–71.
9. Eissa IH, El-Helby A-GA, Mahdy HA, et al. Discovery of new quinazolin-4 (3H)-ones as VEGFR-2 inhibitors: design, synthesis, and anti-proliferative evaluation. Bioorg Chem 2020;105:104380.
10. Ran F, Li W, Qin Y, et al. Inhibition of vascular smooth muscle and cancer cell proliferation by new VEGFR inhibitors and their immunomodulator effect: design, synthesis, and biological evaluation. Oxid Med Cellular Longevity 2021;2021:1–21.
11. Claesson-Welsh L, Welsh M. VEGFA and tumour angiogenesis. J Intern Med 2013;273:114–27.
12. El-Metwally SA, Abou-El-Regal MM, Eissa IH, et al. Discovery of thieno [2, 3-d] pyrimidine-based derivatives as potent VEGFR-2 kinase inhibitors and anti-cancer agents. Bioorg Chem 2021;112:104947.
13. Abbass EM, Khalil AK, Mohamed MM, et al. Design, efficient synthesis, docking studies, and anticancer evaluation of new quinoxalines as potential intercalative Topo II inhibitors and apoptosis inducers. Bioorg Chem 2020;104:104255.
14. Ghorab MM, Alsaid MS, Soliman AM, Ragab FA. VEGFR-2 inhibitors and apoptosis inducers: synthesis and molecular design of new benzo [g] quinazolin bearing benzenesulfonamide moiety. J Enzy Inhib Med Chem 2017;32:893–907.
15. Lee K, Jeong K-W, Lee Y, et al. Pharmacophore modeling and virtual screening studies for new VEGFR-2 kinase inhibitors. Euro J Med Chem 2010;45:5420–7.
16. Machado VA, Peixoto D, Costa R, et al. Synthesis, antiangiogenesis evaluation and molecular docking studies of 1-aryl-3-[(thieno [3, 2-b] pyridin-7-ylthio) phenyl] ureas: Discovery of a new substitution pattern for type II VEGFR-2 Tyr kinase inhibitors. Bioorg Med Chem 2015;23:6497–509.
17. Garofalo A, Goossens L, Six P, et al. Impact of aryloxy-linked quinazolines: A novel series of selective VEGFR-2 receptor tyrosine kinase inhibitors. Bioorg Med Chem Lett 2011;21:2106–12.
18. Elkady H, Elwan A, El-Mahdy HA, et al. New benzoxazole derivatives as potential VEGFR-2 inhibitors and apoptosis inducers: design, synthesis, anti-proliferative evaluation, flowcytometric analysis, and in silico studies. J Enzy Inhib Med Chem 2022;37:397–410.
19. Papaetis GS, Syrigos KN. Sunitinib. Bio Drugs 2009;23:377–89.
20. Soria J-C, DeBraud F, Bahleda R, et al. Phase I/IIa study evaluating the safety, efficacy, pharmacokinetics, and pharmacodynamics of lucitanib in advanced solid tumors. Ann Oncol 2014;25:2244–51.
21. Mahdy HA, Ibrahim MK, Metwaly AM, et al. Design, synthesis, molecular modeling, in vivo studies and anticancer evaluation of quinazolin-4 (3H)-one derivatives as potential VEGFR-2 inhibitors and apoptosis inducers. Bioorg Chem 2020;94:103422.
22. Alanazi MM, Elkady H, Alsaif NA, et al. New quinoxaline-based VEGFR-2 inhibitors: design, synthesis, and antiproliferative evaluation with in silico docking, ADMET, toxicity, and DFT studies. RSC Adv 2021;11:30315–28.
23. Alanazi MM, Eissa IH, Alsaif NA, et al. Design, synthesis, docking, ADMET studies, and anticancer evaluation of new 3-methylquinoxaline derivatives as VEGFR-2 inhibitors and

apoptosis inducers. J Enzy Inhib Med Chem 2021;36: 1760–82.

24. Alanazi MM, Elkady H, Alsaif NA, et al. Discovery of new quinoxaline-based derivatives as anticancer agents and potent VEGFR-2 inhibitors: Design, synthesis, and in silico study. J Mol Struc 2022;1253:132220.

25. El-Zahabi MA, Sakr H, El-Adl K, et al. Design, synthesis, and biological evaluation of new challenging thalidomide analogs as potential anticancer immunomodulatory agents. Bioorg Chem 2020;104:104218.

26. Eldehna WM, Abo-Ashour MF, Ibrahim HS, et al. Novel [(3-indolylmethylene) hydrazono] indolin-2-ones as apoptotic anti-proliferative agents: design, synthesis and in vitro biological evaluation. J Enzy Inhib Med Chem 2018;33:686–700.

27. Al-Rashood ST, Hamed AR, Hassan GS, et al. Antitumor properties of certain spirooxindoles towards hepatocellular carcinoma endowed with antioxidant activity. J Enzy Inhib Med Chem 2020;35:831–9.

28. El-Helby A-GA, Ayyad RR, El-Adl K, Elkady H. Phthalazine-1, 4-dione derivatives as non-competitive AMPA receptor antagonists: design, synthesis, anticonvulsant evaluation, ADMET profile and molecular docking. Mol Div 2019;23: 283–98.

29. El-Helby AGA, Ayyad RR, Zayed MF, et al. Design, synthesis, in silico ADMET profile and GABA-A docking of novel phthalazines as potent anticonvulsants. Archiv Der Pharmazie 2019;352:1800387.

30. Lipinski CA, Lombardo F, Dominy BW, Feeney PJ. Experimental and computational approaches to estimate solubility and permeability in drug discovery and development settings. Adv Drug Del Rev 1997;23:3–25.

31. Veber DF, Johnson SR, Cheng H-Y, et al. Molecular properties that influence the oral bioavailability of drug candidates. J Med Chem 2002;45:2615–23.

32. Alsaif NA, Taghour MS, Alanazi MM, et al. Discovery of new VEGFR-2 inhibitors based on bis ([1, 2, 4] triazolo)[4, 3-a: 3′, 4′-c] quinoxaline derivatives as anticancer agents and apoptosis inducers. J Enzy Inhib Med Chem 2021;36:1093–114.

33. Alsaif NA, Dahab MA, Alanazi MM, et al. New quinoxaline derivatives as VEGFR-2 inhibitors with anticancer and apoptotic activity: design, molecular modeling, and synthesis. Bioorg Chem 2021;110:104807.

34. Wang J, Lenardo MJ. Roles of caspases in apoptosis, development, and cytokine maturation revealed by homozygous gene deficiencies. J Cell Sci 2000;113:753–7.

35. Eldehna WM, Hassan GS, Al-Rashood ST, et al. m. chemistry, Synthesis and in vitro anticancer activity of certain novel 1-

(2-methyl-6-arylpyridin-3-yl)-3-phenylureas as apoptosis-inducing agents. J Enzyme Inhib Med Chem 2019;34:322–32.

36. Lo KK-W, Lee TK-M, Lau JS-Y, et al. Luminescent biological probes derived from ruthenium (II) estradiol polypyridine complexes. Inorg Chem 2008;47:200–8.

37. Sabt A, Abdelhafez OM, El-Haggar RS, et al. Novel coumarin-6-sulfonamides as apoptotic anti-proliferative agents: synthesis, in vitro biological evaluation, and QSAR studies. J Enzyme Inhib Med Chem 2018;33:1095–107.

38. Balah A, Ezzat O, Akool E-S. Vitamin E inhibits cyclosporin A-induced CTGF and TIMP-1 expression by repressing ROS-mediated activation of TGF-β/Smad signaling pathway in rat liver. Inter Immunopharmacol 2018;65:493–502.

39. Aborehab NM, Elnagar MR, Waly NE. Gallic acid potentiates the apoptotic effect of paclitaxel and carboplatin via overexpression of Bax and P53 on the MCF-7 human breast cancer cell line. J Biochem Mol Toxicol 2021; 35:e22638.

40. Elnagar MR, Walls AB, Helal GK, et al. Functional characterization of α7 nicotinic acetylcholine and NMDA receptor signaling in SH-SY5Y neuroblastoma cells in an ERK phosphorylation assay. Euro J Pharmacol 2018;826:106–13.

41. Belal A, Elanany MA, Santali EY, et al. Screening a panel of topical ophthalmic medications against MMP-2 and MMP-9 to investigate their potential in keratoconus management. Molecules 2022;27:3584.

42. Elkaeed EB, Youssef FS, Eissa IH, et al. Multi-step in silico discovery of natural drugs against COVID-19 targeting main protease. Inter J Mol Sci 2022;23:6912.

43. Elkaeed EB, Elkady H, Belal A, et al. Multi-phase in silico discovery of potential SARS-CoV-2 RNA-dependent RNA polymerase inhibitors among 3009 clinical and FDA-approved related drugs. Processes 2022;10:530.

44. Abdallah AE, Alesawy MS, Eissa SI, et al. Design and synthesis of new 4-(2-nitrophenoxy) benzamide derivatives as potential antiviral agents: Molecular modeling and in vitro antiviral screening. N J Chem 2021;45:16557–71.

45. Daina A, Michielin O, Zoete V. SwissADME: a free web tool to evaluate pharmacokinetics, drug-likeness and medicinal chemistry friendliness of small molecules. Sci Rep 2017;7: 42717.

46. Daina A, Michielin O, Zoete V. iLOGP: a simple, robust, and efficient description of n-octanol/water partition coefficient for drug design using the GB/SA approach. J Chem Inform Model 2014;54:3284–301.

47. Lipinski CA, Lombardo F, Dominy BW, Feeney PJ. Experimental and computational approaches to estimate solubility and permeability in drug discovery and development settings. Adv Drug Deliv Rev 2012;64:4–17.